Relic density at one-loop with gauge boson pair production

N. Baro,[1] F. Boudjema,[2] G. Chalons,[2] and Sun Hao[2]

[1]*Institut für Theoretische Physik E, RWTH Aachen University, D-52056 Aachen, Germany*
[2]*LAPTH, Université de Savoie, CNRS, BP 110, F-74941 Annecy-le-Vieux Cedex, France*

We have computed the full one-loop corrections (electroweak as well as QCD) to processes contributing to the relic density of dark matter in the minimal supersymmetric standard model where the lightest supersymmetric particle is the lightest neutralino. We cover scenarios where the most important channels are those with gauge boson pair production. This includes the case of a bino with some wino admixture, a Higgsino and a wino. In this paper we specialize to the case of light dark matter much below the TeV scale. The corrections can have a non-negligible impact on the predictions and should be taken into account in view of the present and forthcoming increasing precision on the relic density measurements. Our calculations are made with the help of SLOOPS, an automatic tool for the calculation of one-loop processes in the minimal supersymmetric standard model. The renormalization scheme dependence of the results as concerns $\tan\beta$ is studied.

I. INTRODUCTION

Existence of nonbaryonic dark matter is established through precise determination of the mean densities of matter in the Universe. However, one does not know what constitutes dark matter even if the measurement of the relic density of cold dark matter is now very precise [1]. On the other hand, the latest observations dedicated to the detection of dark matter have recently received a lot of attention: the PAMELA collaboration has reported a 100 GeV excess on the ratio of fluxes of cosmic ray positrons to electrons [2] and the ATIC balloon experiment claims a cutoff in the positron flux near 500 GeV [3]. The FERMI [4] and HESS [5] observations do not confirm this data but still point to a deviation from the power-law spectrum. Many explanations were advocated to account for these results and the most optimistic and exciting one is that it could be a signal of annihilating dark matter. Supersymmetry can provide, among many other advantages, a dark matter candidate through the lightest supersymmetric particle (LSP) which is a neutralino, $\tilde{\chi}_1^0$, if R-parity is conserved. Meanwhile, the search for dark matter will soon also take place within colliders, in particular, the LHC. If dark matter is discovered among the other new particles that form a new physics model, one will be able to probe its properties. One could then predict the relic abundance of the Universe and would constrain cosmology with the help of precision data [6–8] provided by WMAP [1] and PLANCK [9]. The present WMAP accuracy on the relic density is about 10% and with the PLANCK satellite that has been launched recently it will reach about 2% precision.

Sophisticated codes for the calculation of the relic density in supersymmetry [10–12] exist. However, these codes are essentially based on tree-level cross sections. This is not sufficient to match the foreseen or even the actual accuracy of the relic density. In some of these codes some higher order effects are included, essentially through running of couplings and masses as well as some effective couplings (particularly corrections to the Higgs couplings that can drastically change the results in the so-called Higgs funnel [10]). A couple of recent calculations of loop corrections to the relic density tackled QCD corrections in extreme, though highly interesting, scenarii: annihilation into top quarks at threshold [13] and stop-neutralino coannihilation [14].[1] In [19] QCD corrections to heavy quarks are performed. To match the experimental accuracy, on the theoretical side we have to provide more precise calculations for a much wider class of processes that we encounter in the calculation of the relic density. Therefore we need to evaluate annihilation and coannihilation cross sections at least at next-to-leading order both in α_s (QCD) and α (electroweak corrections). The latter are particular relevant in view of the uncolored nature of dark matter. Considering the very large number of processes required for the evaluation of the relic density and the number of diagrams that each process involves, in particular, at one-loop, automation of the relic density calculations especially in the minimal supersymmetric standard model (MSSM) is unavoidable. Such a program with some applications along these lines was started in [6]. The purpose of this paper is to present some results on the one-loop calculation of the relic density of the LSP in the MSSM, where the dominant annihilation and coannihilation channels are dominated by annihilations into gauge bosons. Beside the physics motivation for such scenarios, calculations of these processes involving gauge bosons are challenging. Attempts to include some effects of the loop

---

[1]We do not list in this category loop induced annihilation processes such as $\tilde{\chi}_1^0 \tilde{\chi}_1^0 \to gg$ [15–18], which contribute very little to the relic density.

corrections through effective couplings for such processes involving gauge bosons are not easy because one has to be careful about maintaining gauge invariance and unitarity. A preliminary study of such scenarios has been made by some of us [6,20]. In this paper we consider the case of a relatively light neutralino. Very heavy neutralinos with TeV masses and above will be studied in a subsequent paper, especially since they show new interesting effects.

The relic abundance will be derived from the assumption that it is thermally produced in the early stages of the universe [21], so in a first approximation the relic density is inversely proportional to the thermal average cross sections, $\langle \sigma v \rangle$. The computations that we present here are performed with the help of SLOOPS [6,22–24], which is a fully automated code for the next-to-leading order calculation of any cross section or decay in the MSSM. Although our main interest concerns the channels with gauge bosons in the final state, we will find that there are non-negligible coannihilations channels with quarks in the final state. We calculate both the electroweak and QCD corrections to these contributions. There can be a host of processes contributing to the relic density for a particular scenario. In this paper we calculate, however, the radiative corrections only to those processes which, at tree-level, contribute more than 5% to the relic density. We study here three different scenarios corresponding to three different compositions of our lightest neutralino: (i) a binolike neutralino with some wino admixture, (ii) a Higgsinolike neutralino, (iii) a light winolike neutralino. We will also study the impact of different choices of the renormalization scheme for $\tan\beta$ on the corrections. To derive the corrected relic density we feed our velocity dependent cross sections into MICROMEGAS [10] for performing the thermal average and solving the Boltzmann equations. We will always show the cross sections (at tree-level and at one-loop) in terms of the relative velocity and as a guide we extract the s-wave and p-wave coefficients and the corrections they receive. This helps also extract the, one-loop, Sommerfeld [25] factor for some of the cross sections. In the processes we study here these are of QED origin. Once these one-loop Sommerfeld QED corrections are extracted we first subtract them before performing the all order resummation and deriving the relic density.

The paper is organized as follows. In the next section we give an overview of SLOOPS and on how we perform the one-loop calculations, in particular, summarizing our renormalization procedure. Checks on the calculations as concerns ultraviolet finiteness, infrared finiteness, and gauge parameter independence are spelled out. The interface between SLOOPS and MICROMEGAS will also be presented. Most of the scenarios that we will be studying involve coannihilation, we will define the effective cross section that includes the statistical weight. At the end of this section we present how our models have been defined. Section III considers the case of a light (about 100 GeV)

mixed bino-wino LSP. The case of a dominantly Higgsino LSP with mass of about 200 GeV is studied in Sec. IV. Section V covers the case of a light wino of about the same mass. The last section contains our conclusions and prospects.

II. OVERVIEW OF THE CALCULATION

A. Set up of the automatic calculation: SLOOPS

One-loop processes calculated via the diagrammatic Feynman approach involve a huge number of diagrams even for $2 \rightarrow 2$ reactions, especially in a theory like supersymmetry. Doing full calculations by hand without automation is practically untractable. There exists already efficient automatic codes for one-loop calculations [26–28]. SLOOPS is an automated code for one-loop calculations in supersymmetry. It is a combination of LANHEP [29], the bundle FEYNARTS [30], FORMCALC [28], and an adapted version of LOOPTOOLS [22,31] (that we will call the FFL bundle from now on). LANHEP deals with one of the main difficulties that has to be tackled for the automation of the implementation of the model file, since this requires that one enters the thousands of vertices that define the Feynman rules. On the theory side, a proper renormalization scheme needs to be set up, which then means extending many of these rules to include counterterms. This part is done through LANHEP, which allows us to shift fields and parameters and thus generates counterterms most efficiently. The ghost Lagrangian is derived directly from the Becchi-Rouet-Stora-Tyutin transformations. The loop libraries used in SLOOPS are based on LOOPTOOLS with the addition of quite a few routines, in particular, those for dealing with small Gram determinants that appear in our case at small relative velocities of the annihilating dark matter, and even more so of relevance for indirect detection [22].

B. Nonlinear gauge fixing

We use a generalized nonlinear gauge [22,32] adapted to the minimal supersymmetric model. The gauge fixing writes

$$\mathcal{L}_{\text{GF}} = -\frac{1}{\xi_W} \left| (\partial_\mu - ie\tilde{\alpha}A_\mu - igc_W\tilde{\beta}Z_\mu)W^{\mu+} \right.$$
$$+ i\xi_W \frac{g}{2}(v + \tilde{\delta}h^0 + \tilde{\omega}H^0 + i\tilde{\kappa}G^0 + i\tilde{\rho}A^0)G^+ \left|^2 \right.$$
$$- \frac{1}{2\xi_Z}\left(\partial_\mu Z^\mu + \xi_Z \frac{g}{2c_W}(v + \tilde{\epsilon}h^0 + \tilde{\gamma}_H^0)G^0\right)^2$$
$$- \frac{1}{2\xi_A}(\partial_\mu A^\mu)^2. \tag{1}$$

Unlike the other parts of the model $\mathcal{L}_{\text{GF}}$ is written in terms of *renormalized* fields and parameters. G^0, $G^\pm$ are the Goldstone fields. We always work with $\xi_{A,Z,W} = 1$ so as to deal with the minimal set of loop tensor integrals. This

implementation of the gauge fixing is very useful to check gauge independence for processes with gauge boson production. More details are given in [23].

C. Renormalization

In our code we have renormalized and implemented each sector of the MSSM. This is explained in detail in [6,23,24]. Here we only briefly sketch the renormalization procedure. We have worked, as far as possible, within an on-shell scheme generalizing what is done for the electroweak standard model [26].

(i) The standard model parameters: the fermion masses as well as the mass of the W and Z are taken as input physical parameters. The electric charge is defined in the Thomson limit, see for example [26]. The light quarks (effective) masses are chosen such as to reproduce the SM value of $\alpha^{-1}(M_Z^2) = 127.77$. This should be kept in mind since one would be tempted to use a $\overline{\text{DR}}$ scheme for α, defined as M_Z, to take into account the fact that dark matter is annihilating at roughly the electroweak scale, so that $\alpha(M_Z^2)$ is a more appropriate choice. We should keep in mind that doing so would amount to correcting the tree-level cross section by about 13% for $2 \rightarrow 2$ processes. As we will see this running does not, most of the time, take into account the bulk of the radiative corrections that we report here.

(ii) The Higgs sector: We take the pseudoscalar Higgs mass M_A as an input parameter and require vanishing tadpoles. $\tan\beta$ is defined through several schemes whose impact on the radiative corrections we will study:

 – a $\overline{\text{DR}}$ definition where the $\tan\beta$ counter-term is defined as a pure divergence leaving out all finite parts.

 – a process-dependent definition of this counterterm by extracting it from the decay $A^0 \rightarrow \tau^+\tau^-$ that we will refer to as $A_{\tau\tau}$ for short. This definition is a good choice for the gauge independence of the processes.

 – an on-shell definition with the help of the mass of the heavy CP Higgs H^0 taken as input parameter called the MH scheme from now on. We have reported elsewhere that this scheme usually introduces large radiative corrections.

These schemes are thoroughly discussed in [23], in particular, the question of gauge invariance of these schemes is addressed.

(iii) The sfermion sector: For the slepton sector we use as input parameters masses of the two charged sleptons which in the case of no-mixing define the R-slepton soft breaking mass, $M_{\tilde{e}_R}$ and the $SU(2)$ mass, $M_{\tilde{e}_L}$, giving a correction to the sneutrino mass at one-loop. In the squark sector each generation needs three physical masses to constrain the breaking parameter $M_{\tilde{Q}_L}$ for the $SU(2)$ part, $M_{\tilde{u}_R}$, $M_{\tilde{d}_R}$ for the R-part. See [24] for details.

(iv) The chargino/neutralino sector: For this sector we implement an on-shell scheme by taking as input three masses in order to reconstruct the underlying parameters M_1, M_2, μ. In SLOOPS [24] the default scheme is to choose two charginos masses $m_{\tilde{\chi}_1^\pm}$ and $m_{\tilde{\chi}_2^\pm}$ as input to define M_2 and μ and one neutralino mass, $m_{\tilde{\chi}_1^0}$, to fix M_1. The masses of the remaining three neutralinos receive one-loop quantum corrections. In this scheme, these counterterms are [24]

$$\delta M_2 = \frac{1}{M_2^2 - \mu^2}\left((M_2 m_{\tilde{\chi}_1^+}^2 - \mu \det X)\frac{\delta m_{\tilde{\chi}_1^+}}{m_{\tilde{\chi}_1^+}}\right.$$
$$+ (M_2 m_{\tilde{\chi}_2^+}^2 - \mu \det X)\frac{\delta m_{\tilde{\chi}_2^+}}{m_{\tilde{\chi}_2^+}} - M_W^2(M_2$$
$$+ \mu s_{2\beta})\frac{\delta M_W^2}{M_W^2} - \mu M_W^2 s_{2\beta}c_{2\beta}\frac{\delta t_\beta}{t_\beta}\Bigg),$$
$$\delta\mu = \frac{1}{\mu^2 - M_2^2}\left((\mu m_{\tilde{\chi}_1^+}^2 - M_2 \det X)\frac{\delta m_{\tilde{\chi}_1^+}}{m_{\tilde{\chi}_1^+}}\right.$$
$$+ (\mu m_{\tilde{\chi}_2^+}^2 - M_2 \det X)\frac{\delta m_{\tilde{\chi}_2^+}}{m_{\tilde{\chi}_2^+}} - M_W^2(\mu$$
$$+ M_2 s_{2\beta})\frac{\delta M_W^2}{M_W^2} - M_2 M_W^2 s_{2\beta}c_{2\beta}\frac{\delta t_\beta}{t_\beta}\Bigg),$$

$$(2)$$

$$\delta M_1 = \frac{1}{N_{11}^{*2}}(\delta m_{\chi_1^0} - N_{12}^{*2}\delta M_2 + 2N_{13}^* N_{14}^* \delta\mu$$
$$- 2N_{11}^* N_{13}^* \delta Y_{13} - 2N_{12}^* N_{13}^* \delta Y_{23}$$
$$- 2N_{11}^* N_{14}^* \delta Y_{14} - 2N_{12}^* N_{14}^* \delta Y_{24}), \qquad (3)$$

with $\det X = M_2\mu - M_W^2 s_{2\beta}$, Y is the neutralino mixing matrix and N its diagonalising unitary matrix, see [24]. Looking at these equations some remarks can be made. First, in the special configuration $M_2 \sim \pm\mu$ an apparent singularity might arise. Reference [6] pinpointed this configuration which can induce a large t_β-scheme dependence in the counterterms $\delta M_{1,2}$ and $\delta\mu$ and therefore to the annihilation of the LSP into W's for a mixed LSP, see also [24]. Second, the choice of $m_{\tilde{\chi}_1^0}$ as an input parameter is appropriate only if the lightest neutralino is mostly bino or if the bino-like neutralino is not too heavy compared to other neutralinos. It is, however, very easy to switch to another scheme or choice of input parameters in the chargino/neutralino sector. For instance, if the bino-like neutralino is the NLSP with mass $m_{\tilde{\chi}_2^0}$, like what occurs in the wino scenario that we study in this paper, we simply take $m_{\tilde{\chi}_2^0}$ as input, in which case

δM_1 is obtained from Eq. (3) by $\delta m_{\chi_1^0} \to \delta m_{\chi_2^0}$ and $N_{1j} \to N_{2j}$.

(v) Finally, diagonal field renormalization is fixed by demanding the residue at the pole of the propagator of all physical particles to be unity, and the non-diagonal part by demanding no-mixing between the different particles when on shell. This is implemented in all the sectors.

(vi) Dimensional reduction is used as implemented in the FFL bundle at one-loop through the equivalent constrained dimensional renormalization [33].

D. Infrared divergences

For the processes $\chi\chi \to XY$, $X, Y = W^\pm, Z^0, f, \ldots$, we can decompose the one-loop amplitudes in a virtual part $\mathcal{M}_{1\text{-loop}}^{\text{EW}}$ (for coannihilation processes with external quarks we also need to add $\mathcal{M}_{1\text{-loop}}^{\text{QCD}}$) and a counter-term contribution $\mathcal{M}_{\text{CT}}$. The sum of these two amplitudes must be ultraviolet finite and gauge independent. Because of the virtual exchange of the massless photon and gluon, this sum can contain infrared divergencies. This is cured by adding a small mass to the photon and/or gluon, λ_γ and λ_g. This is a valid regularization, even for QCD, for all the processes we study here where the non-Abelian nature of QCD does not show up. This mass regulator should exactly cancel against the one present in the final state radiation of a photon (gluon). The QED (QCD) contribution is therefore split into two parts: a soft one where the photon (gluon) energy $E_{\gamma,g}$ is integrated to less than some small cutoff k_c and a hard part with $E_{\gamma,g} > k_c$. The former requires a photon (gluon) mass regulator. Finally, the sum $\mathcal{M}_{1\text{-loop}}^{\text{EW+QCD}} + \mathcal{M}_{\text{CT}} + \mathcal{M}_{\gamma,g}^{\text{soft}}(E_{\gamma,g} < k_c) + \mathcal{M}_{\gamma,g}^{\text{hard}}(E_{\gamma,g} > k_c)$ should be ultraviolet finite, gauge invariant, not depend on the mass regulator and on the cut k_c. We take the strong coupling constant at the electroweak scale $\alpha_s = \alpha_s(M_Z^2) = 0.118$.

E. Checking the result

(i) For each process and set of parameters, we first check the ultraviolet finiteness of the results. This test applies to the whole set of virtual one-loop diagrams. The ultraviolet finiteness test is performed by varying the ultraviolet parameter $C_{\text{UV}} = 1/\varepsilon$, ε is the usual regulator in dimensional reduction. We vary C_{UV} by 7 orders of magnitude with no change in the result. We content ourselves with double precision.

(ii) The test on the infrared finiteness is performed by including both the loop and the soft bremsstrahlung contributions and checking that there is no dependence on the fictitious photon mass λ_γ or gluon mass λ_g.

(iii) Gauge parameter independence of the results is essential. It is performed through the set of the *eight* gauge fixing parameters defined in Eq. (1). The use of the eight parameters is not redundant, as often these parameters check complementary sets of diagrams. It is important to note that in order to successfully achieve this test, one should not include any width in the propagators. However, we encountered a W boson resonance for the calculation of $\chi\chi \to qq'$ and we had to include a width to the W propagator to avoid numerical instabilities; nevertheless, this has been done *only* for the evaluation of the hard emission part and *not* for the virtual and soft part. This will be discussed at more length in due course.

(iv) For the bremsstrahlung part, the soft component is added to the virtual corrections and, for the hard one, we use VEGAS [34] adaptive Monte Carlo integration package provided in the FFL bundle and verify the result of the cross section against COMPHEP [35]. The hard part is also the trickiest, especially when threshold or resonances are encountered as stated above, so for some calculations we use BASES [36] provided in the GRACES package [37], which have a better treatment of singularities [26]. We choose k_c small enough and check the stability and independence of the result with respect to k_c.

F. Effective weighted cross sections

All cross sections σ_{ij} where i, j label the annihilating and coannihilating DM particles i, j can, in general, be expanded in terms of the relative velocity v_{ij}, which for neutralino annihilation is $v = 2\beta = 2\sqrt{1 - 4m_{\tilde\chi_1^0}^2/s}$. Away from poles and thresholds, it is a good approximation to write $\sigma_{ij}v_{ij} = a_{ij} + b_{ij}v^2$, keeping only the s-wave, a_{ij}, and p-wave, b_{ij} coefficients. With T being the temperature, $x = m_{\tilde\chi_1^0}/T$, the thermal average gives

$$\langle\sigma_{ij}v_{ij}\rangle = a_{ij} + 6(b_{ij} - a_{ij}/4)/x. \tag{4}$$

With $g_0 = 2$ the neutralino LSP spin degree of freedom (sdof), the coannihilating particle of sdof g_i and mass m_i contributes an effective relative weight of

$$g_{i,\text{eff}} = \frac{g_i}{g_0}(1 + \Delta m_i)^{3/2}\exp(-x\Delta m_i),$$
$$\Delta m_i = (m_i - m_{\tilde\chi_1^0})/m_{\tilde\chi_1^0}. \tag{5}$$

The total number of sdof is $g_{\text{eff}} = \sum_i g_{i,\text{eff}}$. An approximation to the relic density is obtained through a simple one dimensional integration

$$\Omega h^2 = \left(\frac{10}{\sqrt{g_*(x_F)}} \frac{x_F}{24}\right) \frac{0.237 \times 10^{-26} \text{ cm}^3.\text{s}^{-1}}{x_F J},$$

$$J = \int_{x_F}^{\infty} \langle \sigma v \rangle_{\text{eff}} dx/x^2 \qquad \langle \sigma v \rangle_{\text{eff}} = \sum_{ij} \frac{g_{i,\text{eff}} g_{j,\text{eff}}}{g_{\text{eff}}^2} \langle \sigma_{ij} v_{ij} \rangle.$$

(6)

a_{ij}, b_{ij} that are needed to compute σ_{ij} in Eq. (6) are given in cm^3 s^{-1}. x_F represents the freeze-out temperature. $g_*(x_F)$ is the effective degrees of freedom at freeze-out. g_* is tabulated in MICROMEGAS and we read it, as well as x_F, from there. The weight of a channel (see the percentages we will refer to later) corresponds to its relative contribution to J. We find it instructive to consider the weighted cross section

$$\frac{g_{i,\text{eff}} g_{j,\text{eff}}}{g_{\text{eff}}^2} \sigma_{ij} v_{ij} \qquad (7)$$

By doing this we somehow normalize the contributions of, in particular, the coannihilation cross sections which can be very large compared to the annihilation cross sections, but which at the end do not contribute as much because of the Boltzmann factor, $\exp(-x\Delta m_i)$. In our plots the weight and statistics factors are chosen at freeze-out with $x = x_F$, see Eq. (5), and for ease of notation we drop the label 0000_{eff}. Since $x = x_F$ is the lowest value of x, see Eq. (6), that enters the calculation of the relic density, the weight factor tends to enhance the real contribution of the coannihilation channels. The correct overall weight is in our case given by MICROMEGAS. This fact should be taken into account when we compare the figures where the weighted cross sections are shown and the tables where the overall weight (extracted from MICROMEGAS) is given.

Let us stress once more that in order to derive the relic density we do not rely on the approximations given in Eqs. (4)–(6) but pass all the cross sections to MICROMEGAS.

G. Interfacing SLOOPS with MICROMEGAS

In order to evaluate the relic density, we interfaced SLOOPS with MICROMEGAS to take full advantage of its powerful features concerning the cosmology related part (solving the Boltzmann equations with coannihilation, calculation of the effective degrees of freedom, thermal averaging,...). The connection between the two codes is summarized in the following:

(1) The MSSM default directory of MICROMEGAS uses SUSPECT [38]. In so doing it inherits some of the radiative corrections, in particular, in the spectrum (mass) calculation used in SUSPECT. From the corrected spectrum MICROMEGAS works out new effective tree-level underlying parameters so that gauge invariance is maintained. For the interface we have removed this default option of reading from SUSPECT and created a model file based on the same tree-level Lagrangian as the one used in

SLOOPS. In so doing both SLOOPS and MICROMEGAS calculate the same tree-level cross sections. This is also a check on our tree-level cross sections.

(2) The one-loop cross sections of SLOOPS, appearing into the form of tables showing the cross section as a function of the relative momentum p, $\sigma(p)$, are then interpolated and passed to MICROMEGAS which substitutes these new corrected cross sections to the corresponding tree-level cross sections. Processes that are not corrected (and hence are not substituted) are of course kept in the list of processes for the evaluation of the relic density.

H. Finding scenarios in the MSSM parameter space

The latest limits on the relic density coming from WMAP five years data give the 2σ range [1],

$$0.098 < \Omega_\chi h^2 < 0.122. \qquad (8)$$

When $m_\chi > m_W$, channels with gauge bosons in the final state open and LSP's are annihilating very efficiently, making it difficult to obtain an absolute value of the relic density within the WMAP bounds. In the MSSM this is realized with a neutralino which is mostly winolike or Higgsinolike and its corresponding mass must be around 1 TeV for the latter and 2 TeV in the wino case to be in the cosmologically interesting region. Keeping this in mind we did not worry too much about the value of the relic cosmic abundance and, instead, we restricted ourselves to get gauge bosons in the final state to study the origin of large corrections, if any. Moreover, since the impact of radiative corrections can be large, there is not so much sense in picking up a model based on its agreement with the current data on the basis of a tree-level calculation and finally we could argue that this agreement can be obtained with non-thermal dark matter production, or any other mechanism which could avoid too much depletion. This said, we also wanted to have a rather light spectrum as a supersymmetric solution to the hierarchy problem requires a relatively light LSP and in order to have scenarios testable at colliders. Regardless of these remarks we used MICROMEGAS as a guide, being careful about translations of effective couplings and input parameters.

Last but not least, it is important to stress that we did not apply radiative corrections to all subprocesses but only to the ones contributing more than 5% to the relic density, the remaining ones were included only at tree level. Most often the processes that we do not correct add up to more than 25% of all the processes contributing to the relic density, even if individually their weight is small. Therefore, when calculating the correction to the relic density, the one-loop corrections we compute can get diluted especially if some cancellations occur at one loop between the processes we consider. This point should be kept in mind when we quote the one-loop corrected relic density. Ideally we should

have corrected all cross sections. This could of course be done with our code SLOOPS and interface to MICROMEGAS; however, in these exploratory investigations our aim is to uncover the salient features of the radiative corrections to annihilation and coannihilation of dark matter in supersymmetry.

For all the scenarios we will give below, the low energy tree-level input parameters are defined at the electroweak scale and are: M_1 the $U(1)$ gaugino mass, M_2 the $SU(2)$ counterpart, μ the Higgsino "mass," M_3 the gluino mass, M_A the mass of the pseudoscalar Higgs boson and $\tan\beta$. When not specified, we will take a common sfermion mass. The sfermion trilinear parameter A_f is set to zero for all generations. We do not impose any gaugino mass unification at the GUT scale. Now let us describe the scenarios we study:

(i) Mixed-bino scenario: Usually, assuming gaugino mass universality at the GUT scale leads to a bino-like LSP. This gives a relic density which overcloses the universe. Relaxing this assumption by adding a substantial wino component one can match the WMAP range thanks to the opening of gauge boson channels and coannihilation with $\tilde{\chi}_1^\pm$. This is easily achieved with $M_1 \sim M_2$. In our fist scenario $M_1 \sim 100$ GeV so that the mass of the LSP is around 100 GeV.

(ii) Higgsino scenario: A mainly Higgsino neutralino of mass $m_\chi > m_W$ (here $m_{\tilde{\chi}_1^0} \sim 230$ GeV) will automatically annihilate dominantly into gauge bosons and, because of the degeneracy with the lightest Higgsinolike chargino, coannihilation takes place also.

(iii) Light-wino scenario: A simple way to obtain gauge bosons in the final states of annihilating neutralinos is to increase its $SU(2)$ type coupling by decreasing the value of M_2 in order to have a winolike neutralino whose mass $m_{\tilde{\chi}_1^0}$ is taken around 200 GeV in this case. Once again we have coannihilation of the $\tilde{\chi}_1^0$ with the $\tilde{\chi}_1^\pm$ because of the small mass gap between them.

III. A MIXED BINO SCENARIO

The first example we examine corresponds to a neutralino LSP which has a substantial bino component. It is known that an almost pure bino does not annihilate enough to give the right relic density in the radiation dominated standard scenario. As it couples mostly to particles with largest hypercharge, the R-sleptons, one can increase the LSP annihilation rate by lowering the R-sleptons mass. This is typical of the so-called bulk region of mSUGRA. One can also rely on coannihilation with the next-to-lightest supersymmetric particle (NLSP) to reduce the relic abundance. An example is coannihilation with the $\tilde{\tau}$. We have studied these scenarios in [6] including one-loop

effects. Another solution is to add some wino component by fixing M_2 close to M_1, hence the LSP/NLSP will have strong couplings with the W boson which will dominate the annihilation rate. This is the case we study here. We take chargino masses within the LEP limits while all other particles (sfermions, other neutralinos) are heavy. The underlying parameters of the models are given in Table I.

$M_{1,2}$, μ are reconstructed from $m_{\tilde{\chi}_1^0}$ and $m_{\tilde{\chi}_1^\pm}$, $m_{\tilde{\chi}_2^\pm}$. The relevant physical masses are $m_{\tilde{\chi}_1^0} = 106.9$ GeV, $m_{\tilde{\chi}_1^\pm} = 124.6$ GeV, and $m_{\tilde{\chi}_2^\pm} = 274.8$ GeV. At tree-level $m_{\tilde{\chi}_2^0} = 125.3$ GeV. The neutralino composition is: $\tilde{\chi}_1^0 = 0.94\tilde{B} - 0.20\tilde{W} - 0.27\tilde{H}_1^0 - 0.10\tilde{H}_2^0$, where $\tilde{B}$, $\tilde{W}$, $\tilde{H}_{1,2}^0$ denote the $U(1)$ gaugino or bino, the $SU(2)$ gaugino of wino and the Higgsino, respectively. The wino component is not negligible. As a consequence annihilation into gauge bosons is dominant. The main process $\tilde{\chi}_1^0\tilde{\chi}_1^0 \to W^+W^-$ contributes 44% to the relic density. The important coannihilation channels are $\tilde{\chi}_1^0\tilde{\chi}_1^+ \to Z^0W^+$, $\tilde{\chi}_1^0\tilde{\chi}_2^0 \to W^+W^-$ both contributing 5% and $\tilde{\chi}_1^0\tilde{\chi}_1^+ \to u\bar{d}$ contributing 8%. $\tilde{\chi}_1^0\tilde{\chi}_1^+ \to c\bar{s}$ contributes as much as the $u\bar{d}$ final state. In the following we will refer to only one of these quark final states, of course both are counted for the calculation of the relic density. For the $\tilde{\chi}_1^0\tilde{\chi}_1^+$ coannihilation, the s-channel exchange of a W^+ boson is dominant, see also [39].

Before showing our results, let us comment on a technicality related to the contribution of the hard bremsstrahlung contribution. This concerns the radiative process $\tilde{\chi}_1^0\tilde{\chi}_1^+ \to u\bar{d}\gamma$, see Fig. 1.

As explained above, when charged/colored particles are involved in the initial/final state, initial/final state radiation should be incorporated to have an infrared safe cross section. This emission is split into two pieces, soft and hard, and the cross section must be independent of the cut where these two parts are defined. Calculating the real emission is a tricky task, especially here. Indeed hard photon emission leads to W-return, bringing the intermediate W on-shell, and therefore would lead to numerical instability if no width, Γ_W, is provided for the internal W. We have dealt with this problem by providing a width to the W only when the radiation is hard, as needed. For the soft part, no width is introduced in order to achieve the cancellation of the infrared divergence between the soft bremsstrahlung and the virtual correction where all masses are real. In summary, since the W resonance turns up at an energy much larger than the cutoff energy k_c, where the matching between the soft and hard emission is done, we decided to split the integration on the hard photon phase-space in the $2 \to 3$ process as follows:

TABLE I. Mixed-bino scenario: Values of the first SUSY set of input parameters. Masses are in GeV.

Parameter	M_1	M_2	μ	t_β	M_3	$M_{\tilde{L},\tilde{Q}}$	A_i	M_{A^0}
Value	110	134.5	-245	10	600	600	0	600
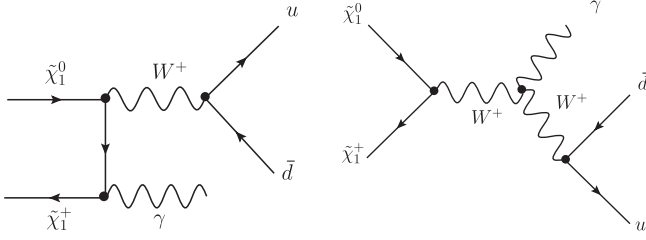
FIG. 1.   Real photon emission leading to W return.

(i) from $k_c < E_{\gamma,g} < \frac{1}{2\sqrt{s}}(s - (M_W^2 + 2\Gamma_W M_W))$,   no width is implemented

(ii) from $\frac{1}{2\sqrt{s}}(s - (M_W^2 + 2\Gamma_W M_W)) < E_{\gamma,g} < \frac{1}{2\sqrt{s}} \times (s - M_{u\bar{d}}^2)$ with a width to the W propagator.

One must note that for (ii) the hard emission is in fact already included in the tree-level process $\tilde{\chi}_1^0\tilde{\chi}_1^+ \to W^+\gamma$ with the W decaying into a $u\bar{d}(, c\bar{s})$ pair. The process $\tilde{\chi}_1^0\tilde{\chi}_1^+ \to W^+\gamma$ contributes to the relic density but we did not added to our list of cross sections to correct as it contributes less than 5%. To avoid double counting when calculating the relic density at one-loop, we therefore subtract from the list of uncorrected tree-level contributions $\tilde{\chi}_1^0\tilde{\chi}_1^+ \to W^+\gamma$ with the proper branching fraction into $u\bar{d}$, $c\bar{s}$. We will encounter this feature for all other scenarios that lead to such a final state and we will treat it in the same way.

Another point is related to processes which are initiated through $\tilde{\chi}_2^0$ coannihilation, $\tilde{\chi}_1^0\tilde{\chi}_2^0 \to W^+W^-$. We are working with a scheme where the input parameters are $m_{\tilde{\chi}_1^0}$, $m_{\tilde{\chi}_1^\pm}$, $m_{\tilde{\chi}_2^\pm}$. Therefore, $m_{\tilde{\chi}_2^0}$ receives a correction at one-loop. In principle, the full one-loop amplitude would write

$$\mathcal{M}_{1\text{-loop}}(m_{\tilde{\chi}_2^0}^{\text{one-loop}}) = \mathcal{M}_{1\text{-loop}}(m_{\tilde{\chi}_2^0})$$
$$+ \Delta m_{\tilde{\chi}_2^0}\frac{\partial \mathcal{M}_{\text{tree}}}{\partial m_{\tilde{\chi}_2^0}}(m_{\tilde{\chi}_2^0}), \qquad (9)$$

where $\mathcal{M}_{\text{tree}}(m_{\tilde{\chi}_2^0})$ is the tree-level amplitude, $m_{\tilde{\chi}_2^0}$ and $m_{\tilde{\chi}_2^0}^{\text{one-loop}} = m_{\tilde{\chi}_2^0} + \delta m_{\tilde{\chi}_2^0}$ is the corrected mass. We have neglected the second contribution. This is because the correction to $m_{\tilde{\chi}_2^0}$ is less than 0.3% for all t_β schemes as shown in Table II. When calculating the relic density we should also, in principle, use the corrected physical mass,

TABLE II.   Mixed-bino scenario: One-loop corrections to the chargino/neutralino masses in GeV in the scheme $m_{\tilde{\chi}_1^0}m_{\tilde{\chi}_1^+}m_{\tilde{\chi}_2^+}$ for different t_β-schemes: $A_{\tau\tau}$, $\overline{DR}$ and MH.

Masses [GeV]		$m_{\chi_2^0}$	$m_{\chi_3^0}$	$m_{\chi_4^0}$
Tree Level		125.3	258.1	270.4
One Loop	- $A_{\tau\tau}$ scheme	125.13	258.58	270.42
	- MH scheme	125.31	258.05	270.65
	- $\overline{DR}$ scheme	125.17	258.46	270.47

like, for example, in the Boltzmann factor, however again this is negligible. Results for the weighted cross sections at tree level and at one loop are displayed in Fig. 2. First of all the QCD and EW corrections to the coannihilation into light quarks add up to about 10% and are practically velocity independent, especially the QCD corrections. The full $\mathcal{O}(\alpha)$ correction to gauge boson production shows the same feature. The dominant annihilation channel into W^+W^- gets about +7% correction, while $\tilde{\chi}_1^0\tilde{\chi}_2^0 \to W^+W^-$ is slightly larger with 9%. $\tilde{\chi}_1^0\tilde{\chi}_1^+ \to Z^0W^+$ is small with about 2%. Had we used a running α at M_Z some of the largest positive corrections would have been absorbed, however our results show that the full corrections are necessary in view of the upcoming precision on the extraction of the relic density. For this scenario, the corrections in the $\alpha(0)$ schemes are positive for all processes we have considered. Nonetheless, since the wino component is important in the evaluation of the cross sections because of the $SU(2)$ quantum numbers of the final states, we expect these results to be sensitive to the $\tan\beta$ scheme, since $\tan\beta$ enters the mixing of the bino and the wino.

Table III gives, in particular, the $\tan\beta$ scheme dependence. As expected the dependence is not negligible, in particular, for the annihilation channel with both LSP in the initial state. The dependence weakens for the coannihilation channels where only one LSP takes part. The M_H scheme is again a bad choice, showing once again [6,23,24] very large corrections. The difference between the $A_{\tau\tau}$ and $\overline{DR}$ is about 2% for the coannihilation channels and 4% for the annihilation channels. At the end taking into account the one-loop corrections only to those processes we studied, which represent 70% off all processes, the correction on the relic density is about -3% in the $A_{\tau\tau}$ scheme and with α defined in the Thomson limit.

IV. LIGHT HIGSSINO SCENARIO

A pure Higgsino state could give an interesting relic density and, as the $\tilde{\chi}_1^0\tilde{\chi}_2^0Z^0$ and $\tilde{\chi}_1^0\tilde{\chi}_1^\pm W^\pm$ are large, annihilates mainly into WW and ZZ final states. Besides, as there are three Higgsinolike states (two neutralinos and one chargino) whose mass splitting is small especially if gaugino masses are large, $m_{\tilde{\chi}_1^0} \simeq m_{\tilde{\chi}_2^0} \simeq m_{\tilde{\chi}_1^\pm} \simeq |\mu|$, coannihilation between the LSP and the other Higgsino states is important. With such efficient annihilations the relic density would be small if the Higgsinolike LSP is too light. Nonetheless, it gives favorable prospects for dark matter direct detection. The scenario we have chosen is described in terms of the underlying parameters given in Table IV.

The LSP neutralino with mass $m_{\tilde{\chi}_1^0} = 234$ GeV has a composition $\tilde{\chi}_1^0 = 0.11\tilde{B} - 0.31\tilde{W} - 0.70\tilde{H}_1^0 - 0.63\tilde{H}_2^0$, indicating it is dominantly a Higgsino state. Coannihilation between the $\tilde{\chi}_1^0$ and $\tilde{\chi}_1^\pm$ occurs since $m_{\tilde{\chi}_1^\pm} = 242.9$ GeV. All other particles, including $\tilde{\chi}_2^0$, are heavy enough and therefore do not take part in the coannihilation.
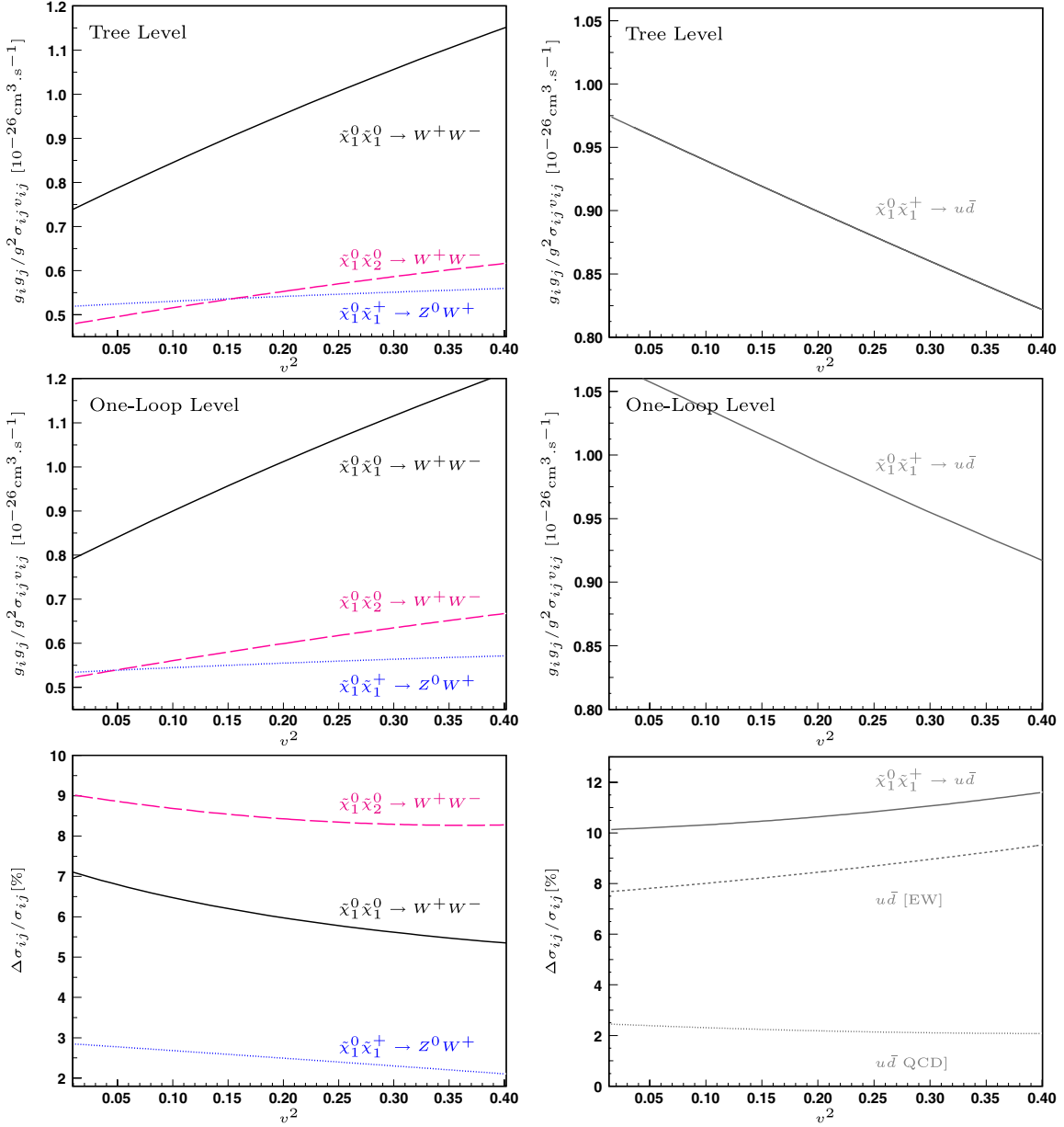
FIG. 2 (color online). Mixed-bino scenario. The left/right panel shows the main gauge boson/quark production cross sections, respectively. All the cross sections are normalised with the corresponding effective degrees of freedom given by Eq. (7) with $x_F = 25.0$. Results are shown for the $A_{\tau\tau}$ scheme of $\tan\beta$.

TABLE III. Mixed-bino scenario: Tree-level values of the *s*-wave (a) and *p*-wave (b) coefficients in units 10^{-26} cm^3 s^{-1}, as well as the relative one-loop corrections in the $A_{\tau\tau}$, $\overline{\rm DR}$, and MH scheme. The percentages in the first column refer to the percentage weight, at tree level, of that particular channel to the relic density.

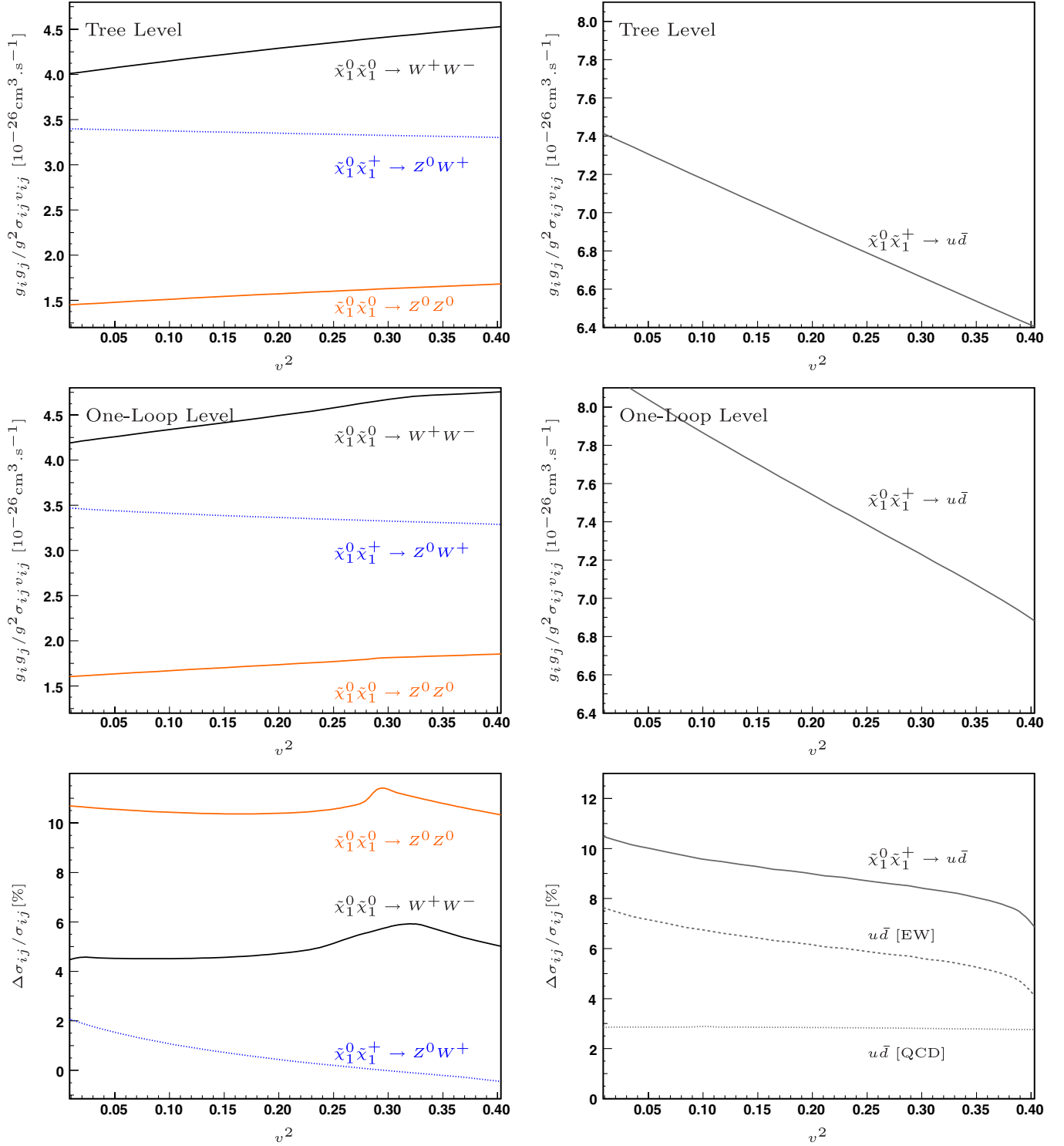|		Tree	$A_{\tau\tau}$	$\overline{\rm DR}$	MH
$\tilde{\chi}_1^0\tilde{\chi}_1^0 \to W^+W^-$ [44%]	a	+0.81	+7.6%	+12.16%	+29.6%
	b	+1.219	+0.78%	+7.1%	+24.2%
$\tilde{\chi}_1^0\tilde{\chi}_1^+ \to u\bar{d}$ [8%]	a	+15.61	+7.2%	+9.8%	+18.8%
	b	−5.81	+5.7%	+8.3%	+17.4%
$\tilde{\chi}_1^0\tilde{\chi}_1^+ \to Z^0W^+$ [5%]	a	+8.26	+2.9%	+4.4%	+9.7%
	b	+1.42	−7.3%	−3.3%	+10.7%
$\tilde{\chi}_1^0\tilde{\chi}_2^0 \to W^+W^-$ [5%]	a	+17.81	+9.0%	+11.1%	+18.2%
	b	+11.86	+4.8%	+7.3%	+16.1%
$\Omega_\chi h^2$		0.108	0.105	0.102	0.097
$\frac{\delta\Omega_\chi h^2}{\Omega_\chi h^2}$			−2.8%	−5.6%	−10.2%

FIG. 3 (color online). Higgsino scenario: The left/right panel shows the main gauge boson/quark production cross sections, respectively. All the cross sections are normalized with the corresponding effective degrees of freedom given by Eq. (7) with $x_F = 27.6$.

As the Higgsino component of the neutralino is important, it will couple mostly to the W and, compared to the mixed bino case, to the Z^0 boson also through the $\tilde{\chi}_1^0 \tilde{\chi}_2^0 Z^0$ coupling.

Dominant tree-level processes relevant for the computation of the relic density are the same as in the previous mixed bino case except for the coannihilation between the first two neutralinos which is Boltzmann suppressed due to

TABLE IV. Higgsino scenario: Parameters defining our Higgsino model with little mixing. Masses are in GeV.

Parameter	M_1	M_2	μ	t_β	M_3	$M_{\bar{L},\bar{Q}}$	A_i	M_{A^0}
Value	400	350	−250	4	1000	650	0	800

their larger mass splitting and smaller couplings. The dominant processes are $\tilde{\chi}_1^0 \tilde{\chi}_1^0 \to W^+ W^-$ contributing (at tree-level) 26% to the relic density, $\tilde{\chi}_1^0 \tilde{\chi}_1^+ \to u\bar{d}(c\bar{s})$ with 12% (12%), $\tilde{\chi}_1^0 \tilde{\chi}_1^0 \to Z^0 Z^0$ with 9% and $\tilde{\chi}_1^0 \tilde{\chi}_1^+ \to Z^0 W^+$ with 6%.

Our results for the cross sections both at tree-level and at one-loop are displayed in Fig. 3. They are shown for $A_{\tau\tau}$ scheme of $\tan\beta$ and where the input for α is in the Thomson limit.

Compared to the mixed bino case, the QCD and EW corrections to coannihilation into light quarks are smaller and no cancellation between the two occurs. The overall correction is almost velocity independent and ranges between 10% to 8%. The corrections to gauge boson production are smaller for $\tilde{\chi}_1^0 \tilde{\chi}_1^0 \to W^+ W^-$ and $\tilde{\chi}_1^0 \tilde{\chi}_1^+ \to Z^0 W^+$ and about 10% for $\tilde{\chi}_1^0 \tilde{\chi}_1^0 \to Z^0 Z^0$. Figure 3 shows a very interesting dynamical effect in the one-loop correction to $\tilde{\chi}_1^0 \tilde{\chi}_1^0 \to W^+ W^-, Z^0 Z^0$ for $v^2 \sim 0.3$. The bumps are in fact due to the opening of the $\tilde{\chi}_1^+$ threshold in the loop, as can be checked explicitly for this value of the velocity and the mass of the LSP compared to that of the $\tilde{\chi}_1^+$. This dynamical structure cannot be described by a simple $a + bv^2$ parametrization of the cross section. Compared to the bino case we have studied in the previous section the $\tan\beta$ scheme dependence is small. The dependence is shown in Table V where we also give the results in terms of the s-wave and p-wave coefficients for a fit in the range $v^2 < 0.3$ so that we avoid the dynamical structure we have just pointed at. The difference between the $A_{\tau\tau}$ scheme and the $\overline{\text{DR}}$ scheme is below 1% for all processes we studied, while the MH scheme gives larger corrections but within

2% compared to the $\overline{\text{DR}}$. For quark production the scheme dependence is even negligible. The overall $\mathcal{O}(\alpha)$ corrections in this scenario, though not negligible, are not that large with α defined in the on-shell scheme in the Thomson limit. Moreover, corrections coming from boxes and final state radiation are often dominant. This suggests that to grab most of the radiative corrections, a full calculation is needed. Within our approach of not correcting the processes that contribute less than 5% to the relic density, the processes we have considered contribute in total only 65%. In this approach we find a correction to the relic density of −2.5% in the $A_{\tau\tau}$ scheme and −2.4% in $\overline{\text{DR}}$. In the MH scheme the correction is little changed to −3.3%.

V. A LIGHT WINO SCENARIO

Models with a light wino as the dark matter candidate occur in theories like AMSB [40], string compactifications [41] and also split-supersymmetry [42,43]. The advantage of a light wino is that it has a large annihilation cross section, relevant for indirect detection, but the main drawback is that it predicts a small thermal relic abundance in the standard cosmological scenario and nonthermal production has to be invoked to recover the correct relic density. The underlying parameters of the model are given in Table VI.

The LSP is now essentially wino with a composition $\tilde{\chi}_1^0 = 0.005\tilde{B} - 0.99\tilde{W} - 0.15\tilde{H}_1^0 - 0.05\tilde{H}_2^0$ and mass $m_{\tilde{\chi}_1^0} = 206.6$ GeV. The LSP is highly degenerate with the $\tilde{\chi}_1^\pm$, their mass difference is $\Delta m \simeq 0.05$ GeV and consequently sizeable coannihilations occur in the determina-

TABLE VI. Light-wino scenario: Values of the fourth SUSY set of input parameters. Masses are in GeV.

Parameter	M_1	M_2	μ	t_β	M_3	$M_{\tilde{u}_L}$	$M_{\tilde{e}_L}$	$M_{\tilde{u}_R,\tilde{e}_R}$	A_i	M_{A^0}
Value	550	210	−600	30	1200	387	360	800	0	700

TABLE V. Higgsino scenario: Tree-level values of the s-wave (a) and p-wave (b) coefficients in units 10^{-26} cm³ s⁻¹ in the Higgsino scenario, as well as the relative one-loop corrections in the $A_{\tau\tau}$, $\overline{\text{DR}}$, MH scheme. The percentages in the first column next to the process refer to the percentage weight, at tree level, of that particular channel to the relic density. The fit into a and b is done in the range $0 < v^2 < 0.3$.

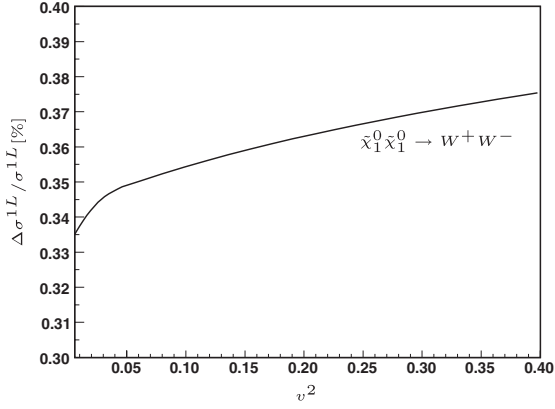|		Tree	$A_{\tau\tau}$	$\overline{\text{DR}}$	MH
$\tilde{\chi}_1^0 \tilde{\chi}_1^0 \to W^+ W^-$ [26%]	a	+11.84	+4.3%	+5.1%	+6.8%
	b	+4.17	+12.7%	+13.4%	+14.9%
$\tilde{\chi}_1^0 \tilde{\chi}_1^+ \to u\bar{d}$ [12%]	a	+15.28	+6.8%	+7.0%	+7.3%
	b	−5.31	+30.4%	+30.7%	+31.3%
$\tilde{\chi}_1^0 \tilde{\chi}_1^0 \to Z^0 Z^0$ [9%]	a	+4.28	+10.4%	+9.6%	+7.8%
	b	+1.83	+12.7%	+12.0%	+10.5%
$\tilde{\chi}_1^0 \tilde{\chi}_1^+ \to Z^0 W^+$ [6%]	a	+6.99	+1.7%	+2.1%	+2.9%
	b	−0.51	+85.6%	+86.5%	+88.4%
$\Omega_\chi h^2$		0.00931	0.00909	0.00908	0.00904
$\frac{\delta\Omega_\chi h^2}{\Omega_\chi h^2}$			−2.4%	−2.5%	−3.3%

FIG. 4. Relative difference for $\tilde{\chi}_1^0\tilde{\chi}_1^0 \to W^+W^-$ between the scheme with $(m_{\tilde{\chi}_1^0}, m_{\tilde{\chi}_1^+}, m_{\tilde{\chi}_2^+})$ and $(m_{\tilde{\chi}_2^0}, m_{\tilde{\chi}_1^+}, m_{\tilde{\chi}_2^+})$ as function of relative velocity. t_β is within the $A_{\tau\tau}$ scheme.
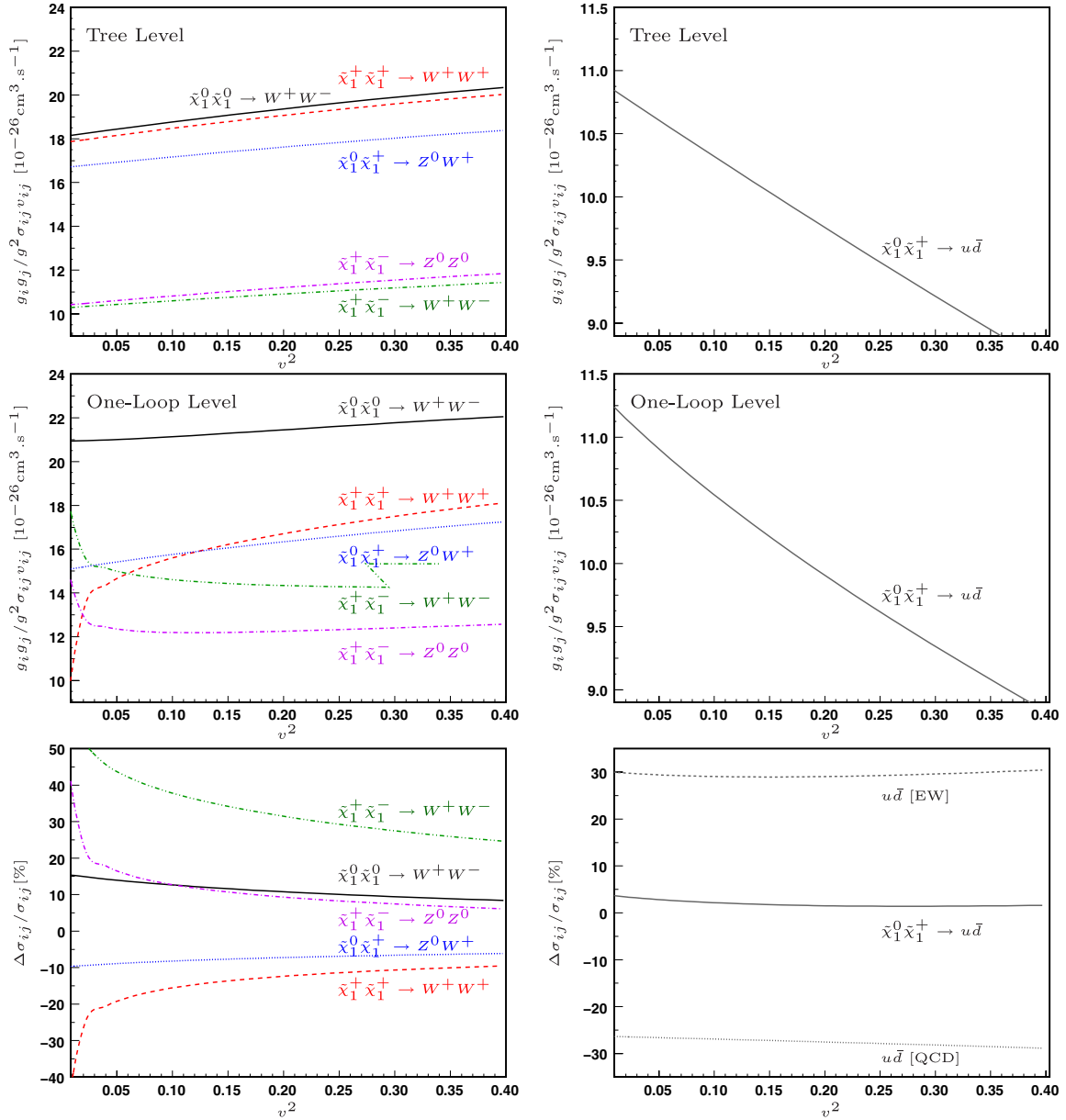

FIG. 5 (color online).   Light-wino scenario: The left/right panel shows the main gauge boson/quark production cross sections, respectively. All the cross sections are normalized with the corresponding effective degrees of freedom given by Eq. (7) with $x_F = 29.9$.

tion of the relic density. With so small of a mass difference, coannihilation processes are important. Products of annihilation/coannihilation processes are into gauge bosons (and some light quarks). The dominant processes are the following: $\tilde{\chi}_1^0\tilde{\chi}_1^0 \to W^+W^-$ [13%], $\tilde{\chi}_1^+\tilde{\chi}_1^+ \to W^+W^+$ [12%], $\tilde{\chi}_1^0\tilde{\chi}_1^+ \to Z^0W^+$ [12%], $\tilde{\chi}_1^+\tilde{\chi}_1^- \to Z^0Z^0$ [7%], $\tilde{\chi}_1^+\tilde{\chi}_1^- \to W^+W^-$ [7%], $\tilde{\chi}_1^0\tilde{\chi}_1^+ \to u\bar{d}$ [7%]. Note in passing that we have taken a large value of $\tan\beta$.

Before we present our results, a word about the renormalization scheme and the choice of input parameters, especially as concerns the neutralino/chargino sector, is in order. The results we will show are based on taking the mass of the LSP as input (beside the masses of the charginos). One might argue that this is not optimal in order to reconstruct the system M_1, M_2, μ, especially for extracting M_1 which is sensitive to the bino-component. One might even expect that at one-loop this scheme would not be suitable since the N_{11} element of the orthogonal matrix in the neutralino sector is very small leading to a large contribution from the counterterm δM_1, see Eq. (3). For this reason, we have been careful in also taking the scheme where the input parameters are $(m_{\tilde{\chi}_2^0}, m_{\tilde{\chi}_1^+}, m_{\tilde{\chi}_2^+})$. Fortunately, as we can see in Fig. 4 for the process $\tilde{\chi}_1^0\tilde{\chi}_1^0 \to W^+W^-$, the difference between the two schemes is within less than 0.4%. We have checked that for other processes in this scenario the difference is also negligible.

The tree-level cross sections and the full one-loop corrections are shown in Fig. 5 as a function of the relative velocity. We note that, at tree-level, these cross sections are *s*-wave dominated. For bosonic final states the velocity dependence is modest, compared to the coannihilation into quarks. For the latter, the electroweak and QCD corrections to $\tilde{\chi}_1^0\tilde{\chi}_1^+ \to u\bar{d}$ are relatively large, of order 30%, but they almost cancel each other. The overall correction is about +5% and practically independent of the velocity. The annihilation process and the $\tilde{\chi}_1^0\tilde{\chi}_1^+$ coannihilation processes show an almost constant correction of order 10%. The coannihilation processes show an interesting behavior in the case where both coannihilating particles are charged, the cross sections reveal a very large correction at very small relative velocity. This correction is the one-loop manifestation of the nonrelativistic Coulomb-Sommerfeld effect [25]. With the tree-level cross section denoted as σ_0 and $\sigma_0 v = a_0 + b_0 v^2$, at vanishing relative velocity the one-loop cross section for chargino annihilation, $\sigma_{\text{Coul}}^{\text{1-loop}}$ is such that

$$\frac{\sigma_{\text{Coul}, v\to 0}^{\text{1-loop}}}{\sigma_0} = \begin{cases} +\frac{\pi\alpha}{v} & \text{for } \tilde{\chi}_1^\pm\tilde{\chi}_1^\mp \\ -\frac{\pi\alpha}{v} & \text{for } \tilde{\chi}_1^\pm\tilde{\chi}_1^\pm. \end{cases}$$

We thus expect the one-loop cross section σ_1 to be

$$\sigma_1 v = a_1 + b_1 v^2 + \pi\alpha c_1/v \quad \text{with} \quad c_1 = \pm a_0. \quad (10)$$

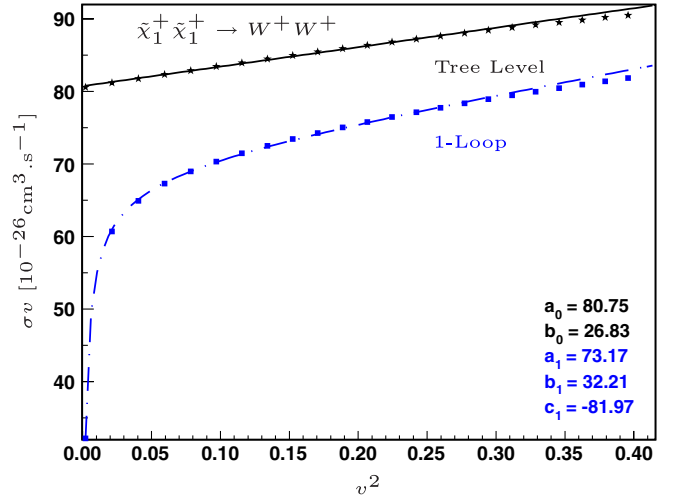To exactly quantify the Sommerfeld effect in our calculation, we have also fitted the one-loop cross section in the

form of Eq. (10). An example of such an exercise is given in Fig. 6 for $\tilde{\chi}_1^+\tilde{\chi}_1^+ \to W^+W^+$. We see therefore that our calculation captures this effect extremely well, indeed we obtain here that $c_1/a_0 = 1.015$ which indeed very close to the analytical result, $c_1/a_0 = 1$. This is important because this effect needs to be summed up to all orders. In our approach we will therefore subtract it from the one-loop correction and replace it by the resummed all order result in the final result. The result of this subtraction on the processes $\tilde{\chi}_1^+\tilde{\chi}_1^- \to Z^0Z^0$, $\tilde{\chi}_1^+\tilde{\chi}_1^+ \to W^+W^+$ and $\tilde{\chi}_1^+\tilde{\chi}_1^- \to W^+W^-$ is shown in Fig. 7.

As one can see once the Coulomb-Sommerfeld contribution is removed, one is left with a smooth cross section, which is almost velocity independent.

FIG. 6 (color online). Light-wino scenario. Fits to the *s*-wave, *p*-wave and Sommerfeld factors for $\tilde{\chi}_1^+\tilde{\chi}_1^+ \to W^+W^+$. In particular, note that the fit in the parametrization of Eq. (10) gives $c_1/a_0 = 1.015$.

The plot shows curves labeled "Tree Level" and "1-Loop" with σv $[10^{-26}\text{cm}^3.\text{s}^{-1}]$ versus v^2, with parameters $a_0 = 80.75$, $b_0 = 26.83$, $a_1 = 73.17$, $b_1 = 32.21$, $c_1 = -81.97$.
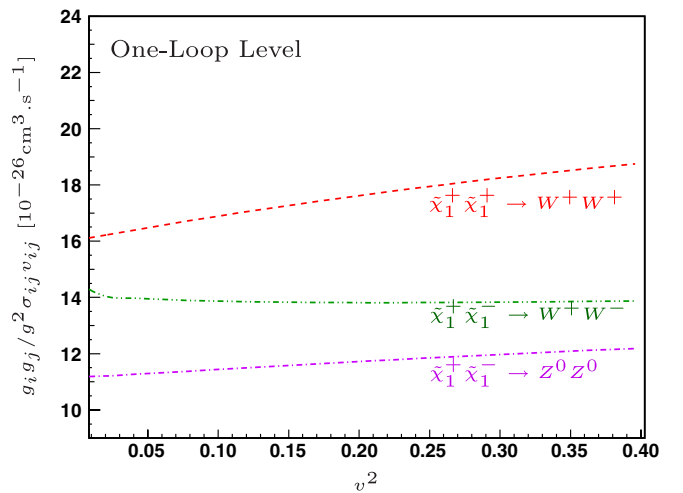

FIG. 7 (color online). Light-wino scenario: Results for one-loop corrections in the $A_{\tau\tau}$ scheme where the QED Sommerfeld effect has been subtracted.

Looking carefully at the results for $\tilde{\chi}_1^+ \tilde{\chi}_1^- \to W^+ W^-$, we note that there is still a slight increase at small v. This is a residual effect of the weak Sommerfeld contribution, see Fig. 8, mediated by a charged W that it is noticeable even for a not too heavy chargino. In fact, a similar effect is also present in $\tilde{\chi}_1^0 \tilde{\chi}_1^0 \to W^+ W^-$. Zooming in on the region of small relative velocity we see a kink, see Fig. 9, around $\sqrt{s} \simeq 413.3$ GeV corresponding to $v \simeq 0.04$, which corresponds to the opening of the threshold of chargino production. In $\tilde{\chi}_1^+ \tilde{\chi}_1^- \to W^+ W^-$ we only see the tail of the opening of the threshold.

Apart from these interesting but numerically small features, let us mention that the t_β scheme dependence is negligible, it is below 0.1%. Our results show that corrections to the individual cross sections can get large at all relative velocities, even after subtracting the QED Sommerfeld effect. For example, $\tilde{\chi}_1^+ \tilde{\chi}_1^- \to W^+ W^-$ gets about +30% correction, while both $\tilde{\chi}_1^+ \tilde{\chi}_1^+ \to W^+ W^+$ and $\tilde{\chi}_1^0 \tilde{\chi}_1^+ \to Z^0 W^+$ get a −10% correction. The dominant cross section $\tilde{\chi}_1^0 \tilde{\chi}_1^0 \to W^+ W^-$ receives a correction of about +15%. The corrections for the other processes are more modest. These corrections are within the on-shell scheme by using $\alpha(0)$. We see that had we used $\alpha(M_Z^2)$ the correction to $\tilde{\chi}_1^0 \tilde{\chi}_1^0 \to W^+ W^-$ would be small, but this is not true for most of the other cross sections where genuine corrections, including hard radiation effects, are important and must be taken into account. This said, when we combine all the cross sections, taking into account their statistical weight, substantial cancellations occur between the different contributions. Add to this that the cross sections we have considered account for about only 65% of all cross sections contributing to the relic density, since we have not considered those contributing individually less than 5%, we find a quite modest (within the $\alpha(0)$ scheme) correction to the relic density of about −2%, see Table VII. This full one-loop correction is practically unchanged if we instead resum the $1/v$ Sommerfeld effect. A similar result was found when we studied $\tilde{\tau}$ coannihilation [6]. This is due to the fact that temperature effects provide a cutoff and the $1/v$ enhancement is tamed after thermal averaging, $\propto \int_0^\infty (dv v^2 e^{-v^2/4x})(\sigma v)$. Our results are summarized in Table VII. The results are presented in terms of the s-wave and p-wave coefficients as well as the Sommerfeld $1/v$ coefficient. The correction to the relic
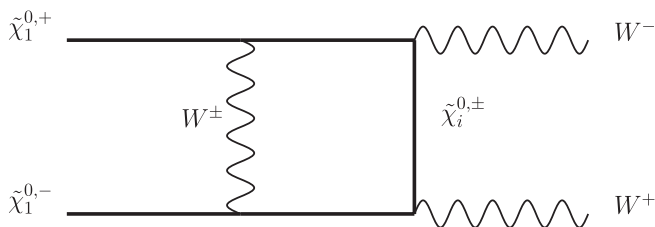

FIG. 8. Example of a box diagram giving rise to the electro-weak equivalent of a Sommerfeld effect.
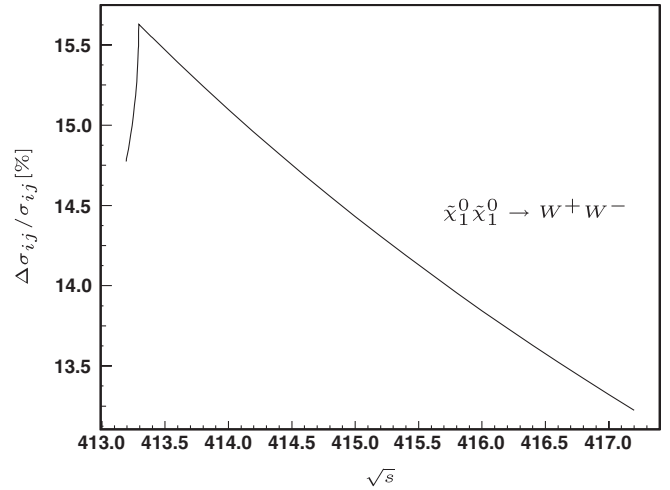

FIG. 9. Light-wino scenario: the kink in $\tilde{\chi}_1^0 \tilde{\chi}_1^0 \to W^+ W^-$ at small relative velocity corresponding to the opening of the threshold for $\tilde{\chi}_1^\pm$ at $\sqrt{s} = 2 \times m_{\tilde{\chi}_1^\pm} = 2 \times 206.646 = 413.3$ GeV.

TABLE VII. Light-wino scenario. The table summarizes the effect of the full order corrections on the dominant processes that contribute more than 5% to the relic density. The relative contribution is given in [ ] next to the process. The tree-level cross sections are given through the fit $\sigma v = a + b v^2$ in the range $0 < v^2 < 0.3$. At the one-loop level, The fitting function is then $\sigma v = a + b v^2 + c \pi \alpha / v$. The coefficients a, b, and c are given units of 10^{-26} cm^3 s^{-1}. The relic density is calculated by taking into account all other processes, which however are not corrected at one-loop. The table also gives the correction after summing the $1/v$ QED contribution at all orders. As the t_β-scheme dependence is less than 0.1%, only one t_β scheme $A_{\tau\tau}$ is presented.

			Tree	Full $\mathcal{O}(\alpha)$
$\tilde{\chi}_1^0 \tilde{\chi}_1^0 \to W^+ W^-$ [13%]		a	+161.8	+14.8%
		b	+53.52	−48.7%
$\tilde{\chi}_1^+ \tilde{\chi}_1^+ \to W^+ W^+$ [12%]		a	+80.75	−9.4%
		b	+26.83	+20.1%
		c		−81.97
$\tilde{\chi}_1^0 \tilde{\chi}_1^+ \to Z^0 W^+$ [12%]		a	+37.50	−9.5%
		b	+10.15	+31.6%
$\tilde{\chi}_1^0 \tilde{\chi}_1^+ \to u \bar{d}$ [7%]		a	+24.44	+3.17%
		b	−12.62	+16.3%
$\tilde{\chi}_1^+ \tilde{\chi}_1^- \to Z^0 Z^0$ [7%]		a	+47.08	+7.1%
		b	+17.71	−29.0%
		c		+47.1
$\tilde{\chi}_1^+ \tilde{\chi}_1^- \to W^+ W^-$ [7%]		a	+46.49	+34.0%
		b	+14.01	−104.4%
		c		+53.34
$\Omega_\chi h^2$			0.002 15	0.002 11
$\frac{\delta \Omega_\chi h^2}{\Omega_\chi h^2}$ 1-loop				−1.9%
$\frac{\delta \Omega_\chi h^2}{\Omega_\chi h^2}$ with resum. Sommerfeld				−1.9%

density is given for the full one-loop, including the one-loop $1/v$ threshold correction, as well as after resumming the $1/v$ contributions. Another word of warning about the interpretation of the corrections in terms of the s-wave and p-wave coefficients (a and b). The corrections to the p-wave coefficients may seem very large here, especially if the corresponding correction to a is large. This is not an indication that the radiative correction on the total cross is very large. Indeed all the cross sections here are s-wave dominated, so that the correction on the s-wave is a good measure of the total correction and when modulated with the statistical weight gives a good approximation to the correction on the relic density.

VI. CONCLUSIONS

Extraction of the relic density will soon provide a measurement of this quantity at the 1% level. On the theoretical side, one must therefore provide a prediction which is at least as precise. In particular, if the particle physics component in terms of computation of the annihilations and coannihilations cross sections are under control, one can indirectly test the cosmology of the Universe. With this precise measurement we can even gain insight into the particle physics model that could be combined with measurements at the colliders. The work in this paper continues the investigations we have made [6] concerning the impact of the radiative corrections on the annihilation and coannihilation cross sections of a neutralino dark matter in the MSSM. Here the emphasis is on processes with dominant gauge boson production channels. We have considered three models with relatively light LSP in the 100–200 GeV range, (i) a dominantly bino with some admixture of wino, (ii) a Higgsinolike and a (iii) winolike LSP. Our study shows that it is not easy to find a general common feature of the radiative corrections. For example, within the same $\tan\beta$ scheme and for relative velocities relevant for the evaluation of the relic density, the dominant process $\tilde{\chi}_1^0\tilde{\chi}_1^0 \to W^+W^-$ gets about 15% correction in the wino case but only 4% in the Higgsino case, while the bino is in between. Also the corrections we have just quoted are within a scheme where the electromagnetic constant is defined at low energy in the Thomson limit. A naive use of $\alpha(M_Z^2)$ would suggest that most of the corrections in the dominant process in the wino case is absorbed, but this would not be true for the other processes nor for the other scenarios. This still does not take into account the effects of

final state radiation. For example, in the same wino scenario, the $\mathcal{O}(\alpha)$ correction to $\tilde{\chi}_1^+\tilde{\chi}_1^- \to W^+W^-$ is large and reaches about 30%. In general the corrections to the different contributing processes for the same scenario can be quite different, in the case of the wino the overall effect on the relic is a cancellation of the corrections between the different processes. With this in mind, and the fact that we did not correct processes that, individually, contribute less than 5% to the relic, we find that the overall effect on the relic is small, -2% in the on-shell scheme with α in the Thomson limit. In this paper we have also pursued our investigation of the effect of the $\tan\beta$ scheme dependence on many observables, not necessarily dark matter annihilation. We confirm once more that the MH scheme is not appropriate while $\overline{\text{DR}}$ and $A_{\tau\tau}$ give generally similar results. In the scenarios we have studied, in fact, the scheme dependence is an issue only for the bino case. This could have been expected as the bino couples to W's only through mixing where $\tan\beta$ is important. We have also uncovered in the case of coannihilation electromagnetic Sommerfeld effects for vanishingly small relative velocity. However, the result of the full one-loop and that of resumming this effect is not noticeable at the level of the relic density evaluation, thermal averaging smooths out the effect. Although the effect is numerically quite small, in the case of the wino we noticed the effect of the electroweak Sommerfeld enhancement. This will become more important for higher wino masses that we will study in another paper. To sum up, it is important to stress that we now have the tools to perform automated calculations relevant for a precise evaluation of the dark matter annihilation cross sections.

[1] J. Dunkley *et al.* (WMAP Collaboration), Astrophys. J. Suppl. Ser. **180**, 306 (2009).

[2] O. Adriani *et al.* (PAMELA Collaboration), Nature (London) **458**, 607 (2009).

[3] J. Chang *et al.*, Nature (London) **456**, 362 (2008).

[4] D. Grasso *et al.*, Astropart. Phys. **32**, 140 (2009).

[5] F. Aharonian *et al.*, arXiv:0905.0105.

[6] N. Baro, F. Boudjema, and A. Semenov, Phys. Lett. B **660**,

550 (2008).

[7] B. C. Allanach, G. Bélanger, F. Boudjema, and A. Pukhov, J. High Energy Phys. 12 (2004) 020.

[8] E. A. Baltz, M. Battaglia, M. E. Peskin, and T. Wizansky, Phys. Rev. D **74**, 103521 (2006).

[9] PLANCK, http://www.rssd.esa.int/index.php?project=PLANCK.

[10] MICROMEGAS: G. Bélanger, F. Boudjema, A. Pukhov, and A. Semenov, Comput. Phys. Commun. **149**, 103 (2002); **176**, 367 (2007); **174**, 577 (2006); http://wwwlapp.in2p3.fr/lapth/micromegas.

[11] DARKSUSY: P. Gondolo *et al.*, J. Cosmol. Astropart. Phys. 07 (2004) 008; http://www.physto.se/~edsjo/darksusy/.

[12] SUPERISORELIC: A. Arbey and F. Mahmoudi, arXiv:0906.0369; http://superiso.in2p3.fr/relic/.

[13] T. Moroi, Y. Sumino, and A. Yotsuyanagi, Phys. Rev. D **74**, 015016 (2006).

[14] A. Freitas, Phys. Lett. B **652**, 280 (2007).

[15] L. Bergström and P. Ullio, Nucl. Phys. **B504**, 27 (1997); arXiv:hep-ph/9706232; Z. Bern, P. Gondolo, and M. Perelstein, Phys. Lett. B **411**, 86 (1997); arXiv:hep-ph/9706538.

[16] F. Boudjema, A. Semenov, and D. Temes, Phys. Rev. D **72**, 055024 (2005); arXiv:hep-ph/0507127.

[17] L. Bergstrom, Phys. Lett. B **225**, 372 (1989); R. Flores, K. A. Olive, and S. Rudaz, Phys. Lett. B **232**, 377 (1989); M. Drees, G. Jungman, M. Kamionkowski, and M. M. Nojiri, Phys. Rev. D **49**, 636 (1994);

[18] V. Barger, W. Y. Keung, H. E. Logan, G. Shaughnessy, and A. Tregre, Phys. Lett. B **633**, 98 (2006).

[19] B. Herrmann and M. Klasen, Phys. Rev. D **76**, 117704 (2007).B. Herrmann, M. Klasen, and K. Kovarik, Phys. Rev. D **79**, 061701 (2009).Phys. Rev. D **80**, 085025 (2009).

[20] N. Baro, G. Chalons, and S. Hao arXiv:0909.3263.

[21] G. Jungman, M. Kamionkowski, and K. Griest, Phys. Rep. **267**, 195 (1996).

[22] F. Boudjema, A. Semenov, and D. Temes, Phys. Rev. D **72**, 055024 (2005).

[23] N. Baro, F. Boudjema, and A. Semenov, Phys. Rev. D **78**, 115003 (2008).

[24] N. Baro and F. Boudjema, Phys. Rev. D **80**, 076010 (2009).

[25] A. Sommerfeld, *Atomic Structure and Spectral lines* (Methuen, London, 1934); L. I. Schiff, *Quantum Mechanics* (McGraw-Hill, New York, 1981), 3rd ed., p. 138; L. Landau et E. Lifchitz, *Mécanique Quantique (T. III)* (Mir, Moscow, 1967), p. 606.

[26] G. Bélanger, F. Boudjema, J. Fujimoto, T. Ishikawa, T.

Kaneko, K. Kato, and Y. Shimizu, Phys. Rep. **430**, 117 (2006).

[27] J. Fujimoto, T. Ishikawa, Y. Kurihara, M. Jimbo, T. Kon, and M. Kuroda, Phys. Rev. D **75**, 113002 (2007).

[28] T. Hahn and M. Perez-Victoria, Comput. Phys. Commun. **118**, 153 (1999); T. Hahn, arXiv:hep-ph/0506201.

[29] A. Semenov, arXiv:hep-ph/9608488; Nucl. Instrum. Methods Phys. Res., Sect. A **389**, 293 (1997); Comput. Phys. Commun. **115**, 124 (1998); arXiv:hep-ph/0208011; Comput. Phys. Commun. **180**, 431 (2009).

[30] J. Küblbeck, M. Böhm, and A. Denner, Comput. Phys. Commun. **60**, 165 (1990); H. Eck and J. Küblbeck, *Guide to FeynArts 1.0* (Würzburg, 1991); H. Eck, *Guide to FeynArts 2.0* (Würzburg, 1995); T. Hahn, Comput. Phys. Commun. **140**, 418 (2001).

[31] T. Hahn, http://www.feynarts.de/looptools/.

[32] F. Boudjema and E. Chopin, Z. Phys. C **73**, 85 (1996).

[33] D. Z. Freedman, K. Johnson, and J. I. Latorre, Nucl. Phys. **B371**, 353 (1992); P. E. Haagensen, Mod. Phys. Lett. A **7**, 893 (1992); F. del Aguila, A. Culatti, R. Muñoz Tapia, and M. Pérez-Victoria, Phys. Lett. B **419**, 263 (1998); Nucl. Phys. **B537**, 561 (1999); **B504**, 532 (1997).

[34] G. P. Lepage, J. Comput. Phys. **27**, 192 (1978).

[35] E. Boos *et al.* (CompHEP Collaboration), Nucl. Instrum. Methods Phys. Res., Sect. A **534**, 250 (2004); A. Pukhov *et al.*, Report No. INP MSU 98-41/542, 1998; http://theory.sinp.msu.ru/comphep/.

[36] S. Kawabata, Comput. Phys. Commun. **41**, 127 (1986); **88**, 309 (1995).

[37] T. Kaneko, in *New Computing Techniques in Physics Research*, edited by D. Perret-Gallix and W. Wojcik (CNRS, Paris, 1990); MINAMI-TATEYA group, KEK Report No. 92-19, 1993; F. Yuasa *et al.*, Prog. Theor. Phys. Suppl. **138**, 18 (2000).

[38] A. Djouadi, J. L. Kneur, and G. Moultaka, Comput. Phys. Commun. **176**, 426 (2007).

[39] H. Baer, A. Mustafayev, E. K. Park, and S. Profumo, J. High Energy Phys. 07 (2005) 046.

[40] L. Randall and R. Sundrum, Nucl. Phys. **B557**, 79 (1999); M. A. Luty, H. Murayama, and R. Rattazzi, J. High Energy Phys. 12 (1998) 027.

[41] B. S. Acharya, K. Bobkov, G. L. Kane, J. Shao, and P. Kumar, Phys. Rev. D **78**, 065038 (2008).

[42] J. D. Wells, Phys. Rev. D **71**, 015013 (2005).

[43] N. Arkani-Hamed and S. Dimopoulos, J. High Energy Phys. 06 (2005) 073; A. Romanino, Nucl. Phys. **B699**, 65 (2004); **B706**, 65(E) (2005); N. Arkani-Hamed, S. Dimopoulos, G. F. Giudice, and A. Romanino, Nucl. Phys. **B709**, 3 (2005).